Paper CIT04-0453

AIRCRAFT ICING SIMULATION USING NAVIER-STOKES AND POTENTIAL FLOW SOLUTIONS FOR THE EXTERNAL AERODYNAMICS

Rafael A. da Silveira
Departamento de Engenharia Mecânica – UFSC, Caixa Postal 476, 88040-000 Florianópolis SC, Brasil
silveira@sinmec.ufsc.br

Clovis R. Maliska
Departamento de Engenharia Mecânica – UFSC, Caixa Postal 476, 88040-000 Florianópolis SC, Brasil
maliska@sinmec.ufsc.br

Diego A. Estivam
Departamento de Engenharia Mecânica – UFSC, Caixa Postal 476, 88040-000 Florianópolis SC, Brasil
estivam@sinmec.ufsc.br

Abstract. *The ice accretion in aircrafts happens when they fly through clouds containing super-cooled water droplets that impinge on the leading edge of the surfaces and freeze, changing the geometry and affecting the aerodynamic characteristics. The mathematical model considers the mass and energy balances for control volumes located over the surface, so that the temperature and the freezing rate can be computed. The mass balance accounts for the impinging water, evaporation, runback and freezing, while the energy balance considers the air and water kinetic heating, evaporative cooling, convection, conduction, sensible energy and latent heat due to phase change. The impinging water flux, heat transfer coefficient, pressure and skin friction are calculated from the external flow solution. In this paper, two approaches are presented. The first considers the potential flow assumption and uses the panel method with boundary layer integration. The water droplets flow is computed by a Lagrangean formulation, in which the droplets trajectories are calculated and the impingement positions provide the collection efficiency. The second approach consists in solving the two-phase (air-water) flow around the geometry by using a two-fluid model implemented in the commercial CFD software CFX (Ansys, Inc. 2003) The key issue of applying the boundary condition for the two phase flow in the commercial software is addressed. In this case, the water impingement flux is provided directly from the flow solution. Ice shapes are obtained by using these two approaches for the external flow solution and are compared for several icing conditions.*

Keywords*. aircraft icing, panel method, two-fluid model, collection efficiency.*

1. Introduction

This paper shows results for ice shapes accreted on the leading edge of an airfoil by solving the external aerodynamics problem with two different methodologies. One considers the external flow as potential and uses the panel method (Hess and Smith, 1967) followed by a boundary layer integration for viscous and heat transfer effects and a Lagrangean "particle-tracking" approach for the water droplets trajectories computation (Silveira, 2001 and Silveira and Maliska, 2001). The other methodology consists in solving the external flow around the airfoil by using the two-fluid model, implemented in the CFX package in which both air and water droplets are treated as continuum phases and the water flux impinging the surface is provided from the flow results at the wall. This model was proposed and used in Silveira et. al (2003).

The external flow solution plays a very important rule in the aircraft icing analysis. This encouraged the development of new methodologies to take into account more physics and to deal with more complex geometries. Earlier works use to consider the first methodology, as in the codes Lewice (Wright, 1995), Canice (Morency et al, 1999) and Trajice2 (Gent, 1994), and in the work of Silveira (2001). In the icing code of ONERA (Hedde et al, 1995), the complete potential flow equation, including compressibility effects, is solved using a finite-difference scheme. All these models use boundary layer integration for thermal and viscous effects and droplets trajectories calculation for collection efficiency. This methodology takes advantage for being relatively simple and fast. However, for complex geometries, especially for 3D cases, the "particle-tracking" approach becomes difficult to implement and is computationally very expensive. Besides, the potential flow assumption is limited to low Mach numbers and low angle of attack.

To deal with complex geometries and flow conditions, the Eulerian-Eulerian approach has been applied successfully for icing analysis. The code Fensap-Ice (Bourgault et al, 2000) computes the two-phase flow by assuming that the droplets do not affect the airflow, therefore, considering them as a passive scalar. A finite element approach is used to solve the transport equations. The work of Naterer (2002) was developed for ice accretion on electricity transmission lines, in which the flow is considered full multiphase, that is, the water droplets are also assumed to affect the airflow. In this case, the same equations solved for the airflow are also solved for the water droplets (disperse

phase). In a recent research, Silveira et al (2003) and Silveira (2004) used the two-fluid model, analogous to Naterer (2002), implemented in the commercial code CFX, to solve the external aerodynamics problem.

External flow results, like collection efficiency, heat transfer coefficient, wall shear stress and pressure distribution at the wall, in addition to the environment conditions, such as velocity, static pressure and static temperature, are the input data for the thermodynamic model. Basically, it consists in carrying out a coupled mass-energy balance in each control volume defined over the surface of the geometry, so that the freezing rate is computed and the ice thickness is obtained for each finite segment defining the surface. This approach is used in Wright (1995) and Silveira and Maliska (2001) and it is based in the work of Messinger (1953).

2. The external flow calculation

This section describes the two approaches used for the external flow computation, the panel method with boundary layer integration and droplets trajectories calculation, and the two-fluid model for the two-phase (air-water) flow around the body. Since the thermodynamic model is two-dimensional, the external flow is computed for 2D geometries, even though the Eulerian approach is formulated for 3D flows.

2.1. The Lagrangean approach

In this methodology, the external flow is considered two-dimensional and solved in three parts: first, pressure and velocity distributions at the wall (potential flow) are computed using the panel method, widely used in aeronautical applications and, therefore, not shown here. A detailed description of such a methodology can be found in Hess (1967) and Silveira (2001). Then, the hydrodynamic and thermal boundary layers are solved by using integral methods. For the hydrodynamic boundary layer, the Kármán-Pohlhausen (Schlichting, 1979) method is applied, where an ordinary differential equation for the momentum thickness is integrated, providing

$$\delta_2(x) = \left(\frac{0.470\upsilon}{U^6} \int_0^x U^5 dx \right)^{\frac{1}{2}} \tag{1}$$

where $U = U(x)$ is the potential flow velocity, provided by the panel method and x is the surface coordinate measured from the stagnation point toward the trailing edge. The wall shear stress is derived from a fourth-order polynomial velocity profile and is given by

$$\tau_0 = \frac{\mu U}{\delta} \left(2 + \frac{\Lambda}{6} \right) \tag{2}$$

where δ is the boundary layer thickness, which is computed from

$$\delta_2 = \frac{\delta}{63} \left(\frac{37}{5} - \frac{\Lambda}{15} - \frac{\Lambda^2}{144} \right) \tag{3}$$

The shape factor Λ is obtained from the solution of a non-linear equation written as

$$\frac{\delta_2{}^2}{\upsilon} \frac{dU}{dx} = \left(\frac{37}{315} - \frac{1}{945}\Lambda - \frac{1}{9072}\Lambda^2 \right)^2 \Lambda \tag{4}$$

For the thermal boundary layer, the Smith-Spalding's method (Schilichting, 1979) is used, in which one has the thermal boundary layer thickness calculated from

$$\delta_t(x) = \left(\frac{46.72\upsilon}{U^{2.87}} \int_0^x U^{1.87} dx \right)^{\frac{1}{2}} \tag{5}$$

In this case, the Nusselt number is given by

$$Nu_c(x) = 2\frac{c}{\delta_t} \tag{6}$$

where c is the cord length of the airfoil. From the Nusselt number, the heat transfer coefficient is readily obtained.

The third part of the external flow calculation is to compute the water droplets trajectories. In this procedure, a droplet is released in a position far enough from the body, where free-stream conditions take place. The droplet is dragged by the airflow, according to the force balance shown in Fig. (1), where $\vec{V_a}$, $\vec{V_p}$ and $\vec{V_\infty}$ are the air, particle (droplet) and free-stream velocities, respectively.
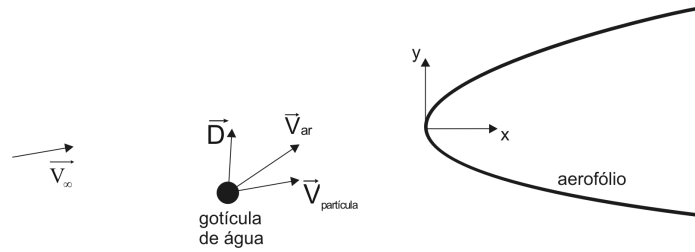

Figure 1: Drag force acting on a water droplet.

The trajectories are then governed by the following equations

$$m \frac{d^2 x_p}{dt^2} = -D \cos \gamma \qquad (7)$$

$$m \frac{d^2 y_p}{dt^2} = -D \sin \gamma \qquad (8)$$

where m is the mass of the droplet and γ is the angle between the droplet and air velocity vectors. The drag force is expressed in terms of a drag coefficient, according to

$$D = c_d \rho_a \frac{V^2}{2} A_p \qquad (9)$$

in which ρ_a is the air density, V is the relative velocity between the air and droplet and A_p is the projected area of the droplet. The drag coefficient is obtained from the Schiller-Naumann correlation (Ansys Inc., 2003 and Silveira et. al, 2003), given by

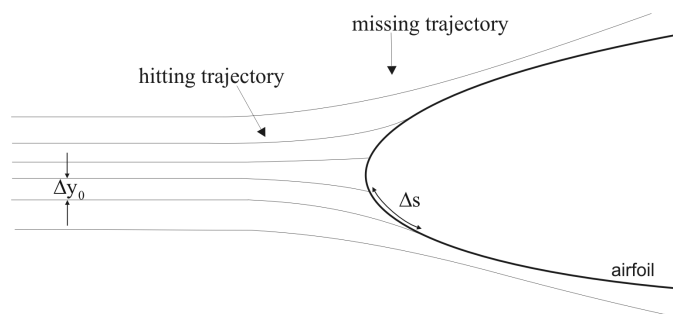$$c_d = \frac{24}{Re_d} \left(1 + 0.15 \, Re_d^{\,0.687} \right) \qquad (10)$$

Figure 2: Droplets trajectories near the airfoil leading edge.

The trajectories are computed until they impinge against the wall or until a pre-defined position in the case when they miss the body. The collection efficiency is the ratio between the wall and free-stream water fluxes, which can be expressed as

$$\beta = \frac{\dot{m}''_{wall}}{\dot{m}''_\infty} \qquad (11)$$

Since the mass flow is constant between two streamlines, one can write

$$\dot{m}_\infty = \dot{m}_{wall} \tag{12}$$

In terms of fluxes, the above relation can be written, according to Fig. (2), as

$$\dot{m}''_\infty \Delta y_0 = \dot{m}''_{wall} \Delta s \tag{13}$$

and the collection efficiency will be given by

$$\beta = \frac{\Delta y_0}{\Delta s} \tag{14}$$

2.2. The Eulerian-Eulerian approach

In this kind of methodology, both air and water droplets are treated as continuum phases, and that transport equations are solved for the two "fluids". Here, the concept of phase volume fraction is introduced, which is the portion of a control volume "filled" by that phase, according to

$$r_i = \frac{V_i}{V} \tag{15}$$

where V_i is the volume occupied by phase i, being i = 1 for the air (continuum phase) and i = 2 for the water (disperse phase).

In this work, as in Silveira, et al (2003) and Silveira (2004), the two-fluid model is used for solving the external flow. In this model, the water droplets (disperse phase) also affect the airflow, differently of the the work of Bourgault et.al (2000) and of the lagrangean approach, where only the influence of the airflow on the water droplets is considered.

By using this concept, the continuity equation for the phase i is written as

$$\frac{\partial(r_i \rho_i)}{\partial t} + \vec{\nabla} \cdot \left(\rho_i r_i \overrightarrow{U_i}\right) = 0 \tag{16}$$

The momentum equation, considering the Reynolds averaging for turbulence, is also solved for each phase and is given by

$$\frac{\partial\left(r_i \rho_i \overrightarrow{U_i}\right)}{\partial t} + \vec{\nabla} \cdot \left(r_i \rho_i \overrightarrow{U_i} \overrightarrow{U_i}\right) = -r_i \vec{\nabla} p'_i + \vec{\nabla} \cdot \left\{ r_i \mu_{eff,i} \left[\vec{\nabla} \overrightarrow{U_i} + \left(\vec{\nabla} \overrightarrow{U_i}\right)^T \right] \right\} + \overrightarrow{S_i} + \overrightarrow{M_i} \tag{17}$$

in which p'_i and $\mu_{eff,i}$ are the pressure and effective viscosity of the phase i, respectively. S_i is related to momentum sources due to external forces (gravity, for example), which are neglected, and M_i represents the interfacial forces. In this work, drag is the only interfacial force to be considered. Then, the drag exerted by the water droplets (i = 2) on the airflow (i = 1) is expressed as

$$\overrightarrow{D_{12}} = \frac{3}{4} \frac{c_d}{d_2} r_2 \rho_1 \left| \overrightarrow{U_2} - \overrightarrow{U_1} \right| \left(\overrightarrow{U_2} - \overrightarrow{U_1}\right) \tag{18}$$

where d_2 is the droplets mean diameter and r_2 is the volume fraction of the phase 2. The drag force acting on the droplets is given by the same expression, except for the volume fraction, which is for the air (r_1). The drag coefficient is given by the same correlation by Shiller-Naumann, as was already mentioned.

The turbulence modeling considers the κ-ε model for the airflow and a zero-equation model for the dispersed phase, where the eddy viscosity is assumed being proportional to the continuum phase eddy viscosity.

The heat transfer problem is governed by the energy equation for multiphase flow, given by

$$\frac{\partial\left(r_i \rho_i c_{p,i} T_i\right)}{\partial t} + \vec{\nabla} \cdot \left(r_i \rho_i c_{p,i} \overrightarrow{U_i} T_i\right) = \vec{\nabla} \cdot \left[\left(r_i k_i + r_i c_{p,i} \frac{\mu_{t,i}}{\sigma_{t,i}}\right) \vec{\nabla} T_i \right] \tag{19}$$

where $c_{p,i}$, k_i, $\mu_{t,i}$ and $\sigma_{t,i}$ are the specific heat, conductivity, eddy viscosity and turbulent Prandl number for the phase i, respectively. There is not available relation for $\sigma_{t,i}$, so the value of 0.9 is usually adopted. In this work, is assumed that the phases share the same temperature field, even though one can consider inter-phase heat transfer. The volume fraction conservation ($r_1 + r_2 = 1$) and the same pressure field for both phases ($p_1 = p_2 = p$) are the closure relations.

The boundary conditions are free-stream flow at INLET boundary and prescribed pressure at the OUTLET boundary, as defined in Fig. (3). The free-stream value for the water volume fraction is obtained from the LWC (Liquid Water Content), which is an environment condition. The WALL boundary is the most complex to deal with, since one wants to compute droplets "impact" velocities on the surface. In the real problem, the water impinging the surface can be seen as "leaving" the domain through the wall, while air flows around the body. To simulate the impingement effect, the wall is treated as an *Outlet* boundary for the disperse phase (water droplets), with no pressure imposed there, and a free-slip wall for the airflow. However, *Outlet* boundary condition may allow flow from the wall to the computational domain (which would be unphysical). Applying zero velocity derivative is not sufficient to represent the correct physical behavior. The procedure adopted here is to compute the normal component of the water velocity vector at the surface. If it "enters" the wall, it set to zero, otherwise it is the correct and it represents the impinging velocity at the wall. Such a condition is named degassing condition and it was implemented in the CFD software CFX (Ansys Inc., 2003) to model free-surface flows of water with air bubbles, and it was first adapted for icing analysis in Silveira et. al (2003).
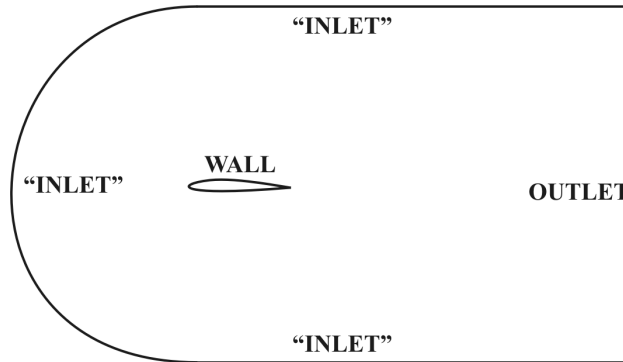

Figure 3: Definitions of the domain boundaries for application of the boundary conditions.

The collection efficiency in the Eulerian approach is computed directly from the flow results. Since β is the ratio between the wall and free-stream water fluxes, as in Eq. (11), one has

$$\beta = \frac{r_2 \vec{V}_2 \cdot \vec{n}_{wall}}{r_{2,\infty} \rho_{2,\infty} |\vec{V}_\infty|} \tag{20}$$

where $\vec{n}_{wall}$ is the unit normal vector at the wall outward the domain and the sub-index 2 refers to water values.

3. The thermodynamic model

The amount of ice accumulated on the leading edge of an aerodynamic surface may be computed by a coupled energy-mass balance in control volumes defined over the external surface, which can be the metallic material or an ice layer, as in the Messinger model (Messinger, 1953). In this work, according to Silveira (2001), the control volumes have the same length of the segments defining the external surface, and the thickness equivalent to the thickness of a water film that would exist if no water were frozen, as in Fig. (4).
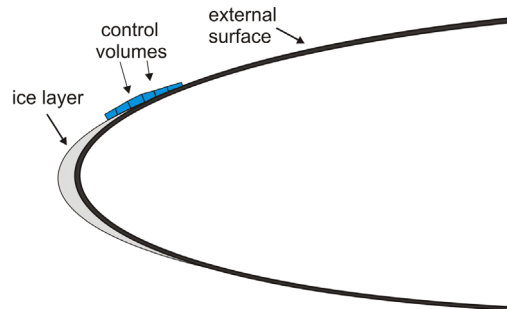

Figure 4: Control volumes over the external surface.

The mass balance accounts for water impingement, evaporation, runback water and freezing, according to Fig. (5). Water droplets freeze immediately when they hit the surface, since they are in a meta-stable equilibrium state. Depending on the surface temperature and the total latent heat released due to freezing, a liquid film lies over the ice

layer or the metallic surface. Then, part of this film can evaporate, flow over the surface (runback water) or freeze in a downstream position.

Balances begin at the control volumes adjacent to the stagnation point, where there is no runback water entering these control volumes, and follow toward the trailing edge through the upper and lower surfaces. The mass balance can be written as

$$\dot{m}''_{rb,in}\delta_s\Delta y + \dot{m}''_{imp}\Delta s\Delta y = \dot{m}''_{evap}\Delta s\Delta y + \dot{m}''_{freeze}\Delta s\Delta y + \dot{m}''_{rb,out}\delta_{s+\Delta s}\Delta y \tag{21}$$

in which Δy is the dimension of the control volume in the span direction of a wing, for example. Since the model is two-dimensional, one can consider $\Delta y = 1$.
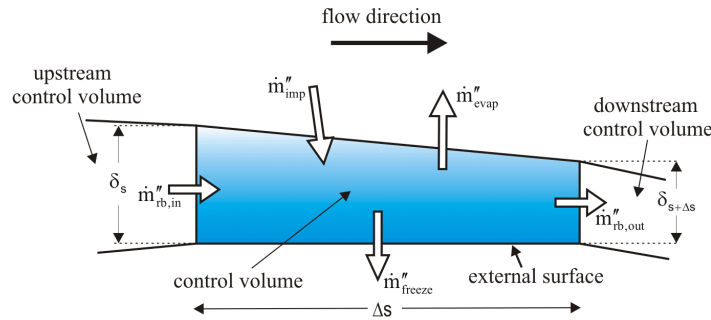

Figure 5: Mass balance in a control volume.

The impingement flux is computed in terms of the collection efficiency as

$$\dot{m}''_{imp} = \beta\, LWC\, U_\infty \tag{22}$$

in which LWC is the liquid water content, which is an environment condition and is an input data for the model. The evaporation flux is related to concentration and temperature gradients across the boundary layer and it is expressed as

$$\dot{m}''_{evap} = \frac{h}{c_{p,air}}\frac{Mw_{water}}{Mw_{air}}Le^{-\frac{2}{3}}\left[\frac{p_{v,\infty}}{p_\infty}r_h - \frac{p_{v,s}}{p_o}\frac{T_o}{T_s}\left(\frac{p_o}{p}\right)^{\frac{1}{\gamma}}\right] \tag{23}$$

in which h is the heat transfer coefficient, Mw is the molecular weight, Le is the Lewis number, r_h is the relative humidity (input data) and p_v is the vapor pressure. The sub-index "s" means the surface and "o" is related to stagnation properties. More details about this term can be found in Silveira (2001), Silveira and Maliska (2001) and Wright (1995).

The freezing flux is computed by defining the freezing fraction, which is the fraction of water that freezes in the control volume and it is obtained from the enthalpy formulation for phase change problems (Silveira, 2004) as

$$f_s = \frac{T_m + \Delta T_m - T}{2\Delta T_m} \tag{24}$$

in which T_m is the melting temperature of ice (273.15 K) and ΔT_m is a range around the melting temperature in which the water is assumed to freeze. Then, the freezing flux is given by

$$\dot{m}''_{freeze} = f_s\left(\dot{m}''_{imp} + \dot{m}''_{rb,in}\right) \tag{25}$$

Since there is no runback water entering the control volume adjacent to the stagnation point, the mass balance can be written for the runback flow leaving the control volume in the form

$$\dot{m}_{rb,out} = \dot{m}_{rb,in} + \left(\dot{m}''_{imp} - \dot{m}''_{evap} - \dot{m}''_{freeze}\right)\Delta s \tag{26}$$

The runback water leaving a control volume will be the runback water entering the next control volume. The film thickness and the film average velocity can be computed by assuming a linear velocity profile and applying zero velocity at the wall and momentum flux continuity at the interface with the external flow (Silveira, 2004).

Some of the terms in the mass balance depend on the control volume temperature, which is assumed being the surface temperature. This temperature is obtained from an energy balance in the same control volume used for the mass balance, according to Fig. (6).
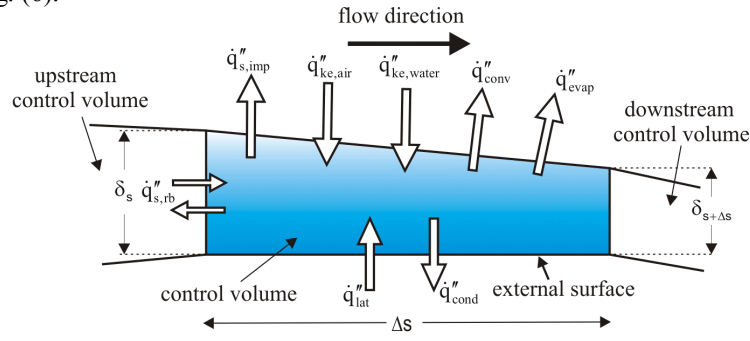

Figure 6: Energy balance in the control volume.

The energy balance accounts for sensible heat lost to the impinging droplets ($\dot{q}''_{s,imp}$), sensible heat transfer due to runback water ($\dot{q}''_{s,rb}$), kinetic heating from the airflow ($\dot{q}''_{ke,air}$), kinetic heating due to droplets impact ($\dot{q}''_{ke,water}$), convection heat losses ($\dot{q}''_{conv}$), evaporative cooling ($\dot{q}''_{evap}$), conduction into the metal or ice layer ($\dot{q}''_{cond}$) and latent heat released during solidification ($\dot{q}''_{lat}$). Then, it can be written as

$$\dot{q}''_{ke,air}\Delta y \Delta s + \dot{q}''_{ke,water}\Delta y \Delta s + \dot{q}''_{lat}\Delta y \Delta s + \dot{q}''_{evap}\Delta y \Delta s + \dot{q}''_{cond}\Delta y \Delta s + \dot{q}''_{conv}\Delta y \Delta s + \dot{q}''_{s,imp}\Delta y \Delta s + \dot{q}''_{s,rb}\delta_s \Delta y = 0 \qquad (27)$$

where each heat flux already has its correct signal. The kinetic heating due to friction from the airflow, kinetic heating due to droplets impact and the heat lost by convection are given respectively by

$$\dot{q}''_{ke,air} = h(T_r - T_\infty) \qquad (28)$$

$$\dot{q}''_{ke,water} = \dot{m}''_{imp}\frac{U^2_{w,imp}}{2} \qquad (29)$$

$$\dot{q}''_{conv} = h(T_s - T_\infty) \qquad (30)$$

where $U_{w,imp}$ is the water impact velocity at that position, T_∞ is the free-stream temperature, T_s is the surface temperature and T_r is the recovery temperature. The latent heat released during the solidification and the evaporative cooling depend on the freezing flux and evaporation mass flux, respectively, and are expressed as

$$\dot{q}''_{lat} = \dot{m}''_{freeze}h_{sl} \qquad (31)$$

$$\dot{q}''_{evap} = \dot{m}''_{evap}h_{lv} \qquad (32)$$

where h_{sl} and h_{lv} are the latent heats of solidification and evaporation of water, respectively.

The metallic layer, as well as the ice layer, when it exists, is treated as a semi-infinite solid (Incropera, 1998), for the conduction heat flux one has

$$\dot{q}''_{cond} = -k\frac{T_r - T_s}{\sqrt{\pi\alpha t}} \qquad (33)$$

where k and α are the thermal conductivity and thermal diffusivity of the metallic material or the ice, respectively. Since this term is time dependent, a time-integrated average value is used in the simulation.

Finally, the sensible heat due to the runback water depends on the surface temperature according to

$$\dot{q}''_{s,rb} = \dot{m}''_{rb,in}c_{p,water}(T_{rb,in} - T_m) + \dot{m}''_{rb,in}c_{p,ice}(T_m - T_s), \text{ if } T_s < T_m \qquad (34)$$

$$\dot{q}''_{s,rb} = \dot{m}''_{rb,in}c_{p,water}(T_{rb,in} - T_s), \text{ if } T_s \geq T_m \qquad (35)$$

where $T_{rb,in}$ is the runback temperature (temperature of the upstream control volume). For the sensible heat lost due to the impinging droplets entering the control volume, the expression is analogous, therefore

$$\dot{q}''_{s,imp} = \dot{m}''_{imp} c_{p,water} \left(T_\infty - T_m \right) + \dot{m}''_{imp} c_{p,ice} \left(T_m - T_s \right), \text{ if } T_s < T_m \tag{36}$$

$$\dot{q}''_{s,imp} = \dot{m}''_{imp} c_{p,water} \left(T_\infty - T_s \right), \text{ if } T_s \geq T_m \tag{37}$$

The energy balance is solved for the control volume temperature by using an iterative method (Newton-Raphson in this work). For each iteration, and temperature correction, the mass balance is recomputed to account for the temperature change.

The result of the balances is the freezing flux, which is used to compute the ice thickness for each segment of the external surface, by assuming that the freezing flux is constant along a time step, according to

$$\varepsilon_{ice} = \frac{\dot{m}''_{freeze} \Delta t}{\rho_{ice}} \tag{38}$$

The procedure consists in solving the external surface for the clean geometry, computing the ice thickness for a pre-defined time interval by applying the thermodynamic model, and changing the surface by adding the ice thickness. The external flow is solved again for this new geometry and another ice layer is added. The procedure is repeated until the desired time. A more detailed description of the thermodynamic model can be found in Silveira (2001), Silveira and Maliska (2001) and Wright (1995).

4. Results

In this section, some results for ice accretion on airfoils are presented by using the two approaches described for the external flow calculation. Table (1) summarizes the flow conditions for the simulations. For cases 1 to 3, ice shapes provided by these two formulations are compared with experimental and simulated results provided by the Lewice code, all of them available in Wright et. al (1997). For cases 4 to 6, the ice profiles are compared with experimental obtained from Addy Jr. (2000). The results are denoted by "Aeroicing Lagr." for the external flow solved with the Lagrangean formulation and with "Aeroicing CFX" when it is done with the Eulerian approach. The first two cases are for rime ice, where there is no runback water and all of the water impinging the body freezes. The other cases are for glaze ice conditions, in which there is some runback water flowing over the surface, so that the thermodynamic behavior of the system is more complex.

Table 1: Summary of simulated cases.

Cases	1	2	3	4	5	6
Airfoil	NACA 0012	NACA 0012	NACA 0012	Business jet	Business jet	Business Jet
Chord(m)	0.5334	0.5334	0.5334	0.9144	0.9144	0.9144
AOA (°)	4	4	4	6	1.5	6
V$_\infty$ (m/s)	58.1	93.8	58.1	90.02	128.61	90.02
T$_\infty$ (K)	245.2	242.5	266.3	268.15	262.95	266.95
P$_\infty$ (kN/m^2)	95.61	92.06	95.61	117.21	200.64	195.12
MVD (μm)	20	20	20	20	20	15
LWC (g/m^3)	1.3	1.05	1.3	0.54	0.54	1.0
Time (min)	8	6.2	8	6	6	15

Figure 7 and Fig. (8) show results for the rime ice simulations (cases 1 and 2). For these cases, the free-stream temperature is lower and all of the water impinging the surface freezes, so that the mass balance reduces to the impingement and freezing fluxes. The profiles point out that the methodologies for the external flow calculation are equivalent for these cases, since the ice shapes and ice mass depend directly on the collection efficiency, which is being correctly calculated.

For cases 3 to 6, shown in Fig. (9) to Fig. (12), one has glaze ice conditions, in which a part of the impinging water does not freeze and flows over the surface. The runback water may freezes at downstream positions, giving rise to the "ice horns". Glaze ice occurs for free-stream temperatures closer to the phase change temperature and the heat transfer coefficient is very important in the heat balance. The results show that the Eulerian approach provides better ice shapes than the Lagrangean approach does for theses cases, as a consequence of a more accurate heat transfer coefficient calculation. Figure 10 shows that the Lagrangean approach yields a better fitting with the experimental profile for case

4, especially in the "ice horn" region. However, it can be observed that the amount of ice is better predicted by the Eulerian approach. In the other cases, the Eulerian approach predicts both shape and amount of ice better than the Lagrangean does.

The difference in results can be attributed principally to the boundary layer transition prediction. The Navier-Stokes equations, associated with a good turbulence model (SST was used in this work) can provide good transition process, while the integral methods depend on prescribing a transition point or computing a value based on some criteria (Reynolds number based on the wall roughness was used in this work).
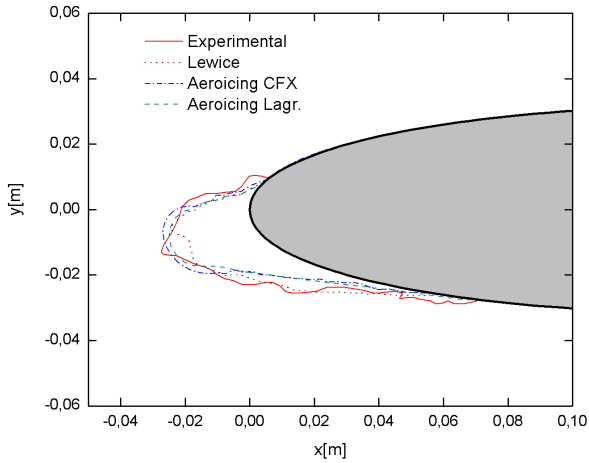
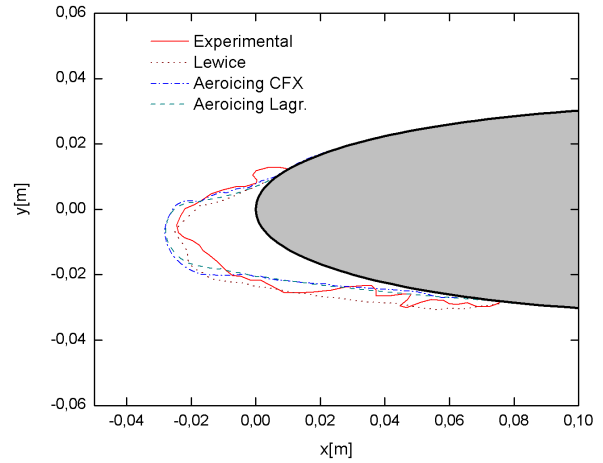Figure 7: Ice shapes results for case 1.
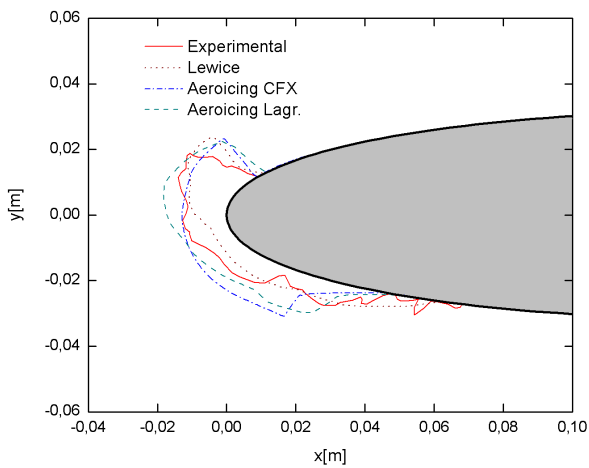

Figure 8: Ice shapes results for case 2.

Figure 9: Ice shapes results for case 3.

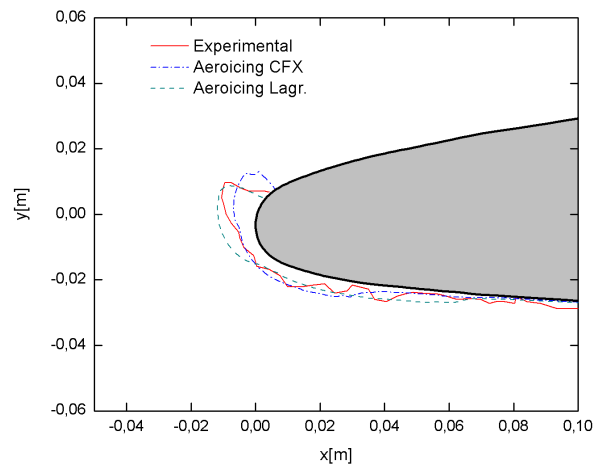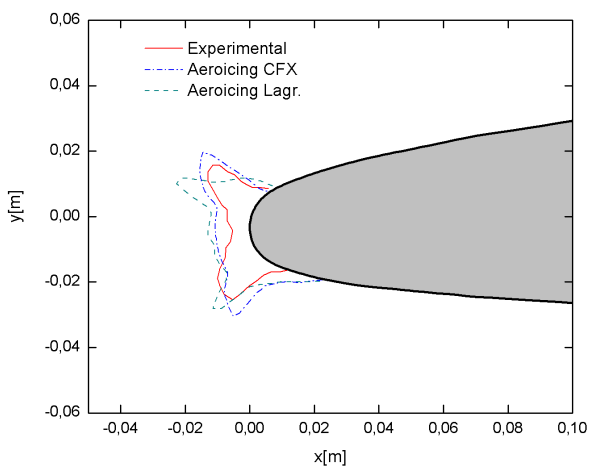
Figure 10: Ice shapes results for case 4.
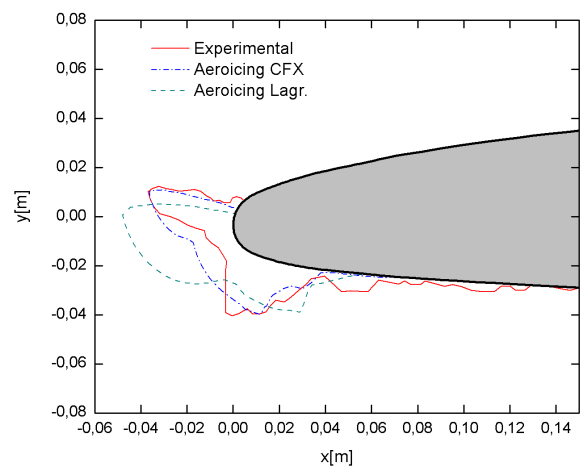

Figure 11: Ice shapes results for case 5.

Figure 12: Ice shapes results for case 6.

5. Concluding remarks

This paper has shown the predictions of ice shapes obtained with two approaches for the external flow calculation. The results show that the Eulerian approach can provide better results than the Lagrangean approach in glaze ice conditions. However, the two-fluid model requires much more computational effort related to panel method with boundary layer integration and "particle-tracking" for simple 2D geometries. For 3D geometries, the Eulerian approach is more suitable, since the water mass flux impinging the surface is computed directly from the flow solution. In the case of particle-tracking approach, the impingement position of each droplet must be computed, which is a very difficult process for complex geometries.

The boundary condition for the water droplets in the Eulerian approach (implemented in the CFX software), advanced in Silveira, et al (2003) was successfully applied and can be still explored to yield even better results. The weak point of this formulation is the high computational cost, since one has to compute the airflow with no-slip condition at wall, for the shear stress computation, and then solve the two-phase flow to obtain the collection efficiency. Effort has been dedicated to change this boundary condition in the software for considering a no slip-wall condition for the continuous phase (Silveira, 2004).

6. References

Addy Jr., H.E., 2000, "Ice Accretion and Icing Effects for Modern Airfoils", NASA/TP 2000 – 210031.

Ansys Inc., 2003, "CFX 5.6 User´s Manual.

Bourgault, Y., Habashi, W. G., Dompierre, J. and Baruzzi, G.S., 1999, "A Finite Element Method Study of Eulerian Droplets Impingement Models", International Journal for Numerical Methods in Fluids, v. 29, pp. 429-449.

Gent, R.W. and Gent, R.W., 1994, "TRAJICE2 - A Combined Water Droplet Trajectory and Ice Accretion Prediction Code for Aerofoils," RAE-TR-90054.

Hedde, T. and Guffond, D., 1995, "ONERA Three-Dimensional Icing Model", AIAA Journal, v. 33, n. 6, pp. 1038-1045.

Hess, J.L., and Smith, A.M.O., 1967 "Calculation of Potential Flow About Arbitrary Bodies", Progress in Aeronautical Sciences, 8: 1–138, (D. Kuchemann, editor), Elmsford, New York, Pergmon Press.

Messinger, B.L., 1953, "Equilibrium Temperature of an Unheated Icing Surface as a Function of Air Speed". Journal of the Aeronautical Sciences, pp. 29-42.

Morency, F., Tesok, F. and Paraschivoiu, I., 1999, "Anti-Icing Simulation Using CANICE", Journal of Aircraft, v. 36, n. 6.

Naterer, G.F., 2002, "Multiphase Flow with Impinging droplets and Airstream Interaction at a Moving Gas/Solid Interface", International Journal of Multiphase Flow, v. 28, pp. 451-477.

Schlichting, H., 1979, "Boundary-Layer Theory", New York: Mc Graw Hill, Inc., ed. 7.

Silveira, R. A., 2001, "Simulação Numérica da Formação de Gelo na Borda de Ataque de Perfis Aerodinâmicos", MSc Thesis, in Portuguese, Departamento de Engenharia Mecânica, Universidade Federal de Santa Catarina, Florianópolis, SC, Brasil.

Silveira, R. A., and Maliska, C.R., 2001, "Numerical Simulation of Ice Accretion on the Leading Edge of Aerodynamic Profiles", in Computational Heat and Mass Transfer-CHMT 2001, pp. 33-40, J. Pontes, Ed., E-Papers Publishing House Ltd., Rio de Janeiro.

Silveira, R. A., Maliska, C.R., Estivam, D.A. e Mendes, R., 2003, "Evaluation of Collection Efficiency Methods for Icing Analysis", Anais do XVII COBEM – International Congress of Mechanical Engineering, São Paulo – SP.

Silveira, R. A., 2004, "Previsão Tridimensional da Formação de Gelo em Superfícies Aerodinâmicas", PhD Thesis Proposal, in Portuguese, Departamento de Engenharia Mecânica, Universidade Federal de Santa Catarina, Florianópolis, SC, Brasil.

Wright, W. B., 1995, "Users Manual for the Improved NASA Lewis Ice Accretion Code Lewice 1.6", NASA CR – 198355.

Wright, W. B., Gent, R. W. and Guffond, D., 1997, "DRA/NASA/ONERA Collaboration on Icing Research Part II – Prediction of Airfoil Ice Accretion", NASA CR – 202349